1-1-2008

Evaluation of photodynamic therapy-induced edema in the rat brain using magnetic resonance imaging

David Chighvinadze
University of Nevada, Las Vegas

EVALUATION OF PHOTODYNAMIC THERAPY-INDUCED EDEMA IN THE RAT BRAIN USING MAGNETIC RESONANCE IMAGING

by

David Chighvinadze

Bachelor of Sciences in Physics
Ivane Javakhishvili State University of Tbilisi
Republic of Georgia
2003

Master of Science in Physics
Ivane Javakhishvili State University of Tbilisi
Republic of Georgia
2005

A thesis submitted in partial fulfillment
of the requirements for the

Master of Science Degree in Health Physics
Department of Health Physics
Division of Health Sciences

Graduate College
University of Nevada, Las Vegas
August 2008

UNLV
UNIVERSITY OF NEVADA LAS VEGAS

Thesis Approval

The Graduate College
University of Nevada, Las Vegas

July 23, 2008

The Thesis prepared by

David Chighvinadze

Entitled

Evaluation of Photodynamic Therapy-Induced Edema In The Rat Brain Using Magnetic Resonance Imaging

is approved in partial fulfillment of the requirements for the degree of

Master of Science in Health Physics

Examination Committee Chair

Dean of the Graduate College

Examination Committee Member

Examination Committee Member

Graduate College Faculty Representative

ABSTRACT

Evaluation of photodynamic therapy-induced edema in the rat brain using magnetic resonance imaging

by

David Chighvinadze

Dr. Steen Madsen, Examination Committee Chair
Chair of the Department of Health Physics
University of Nevada, Las Vegas

Failure of treatment for high-grade gliomas is usually due to local recurrence at the site of surgical resection indicating that a more aggressive form of local therapy should be used. Photodynamic therapy (PDT) shows promising results in the treatment of gliomas as it has been shown to cause significant destruction of tumor cells through localized necrosis and/or apoptosis. An unfortunate complication of this therapy is the induction of cerebral edema which causes increased intracranial pressure and associated morbidity. A potential solution is the administration of steroids to reduce PDT-induced edema, associated morbidity, and mortality in treated animals. In the research described here, high field strength (3 T) magnetic resonance imaging (MRI) was used for screening and detecting the extent and time evolution of PDT-induced edema. Results using inbred Fischer 344 rats subjected to PDT showed that this noninvasive imaging technique was very useful for studying and evaluating treatment-induced edema, its dependence on the PDT light fluence, and the effects of steroids. The data suggest that higher light fluences cause greater edema formation and higher mortality, while the addition of postoperative

steroid treatment reduces the incidence of treatment-induced morbidity and mortality. The images also provided information about blood-brain barrier patency, which is important in therapeutic regimens involving the delivery of drugs (e.g. chemotherapeutic agents) to the brain. PDT appeared to open the BBB for a period of 24-48 hours after which it was restored.

TABLE OF CONTENTS

LIST OF FIGURES

ACKNOWLEDGMENTS

A very special thanks to my advisor Dr. Steen Madsen. I am grateful to him as he always gave me support, guidance and excellent advice during my study and research here at UNLV.

I want to thank my thesis committee members: Dr. Phillip Patton, Dr. Henry Hirshberg, Dr. Ralf Sudowe, and Dr. Merrill Landers. I am honored to have this group of scientists in my committee.

I also want to thank Doris Coomes, Dennis Farmer and Mary Turner for all their help and support over the years.

This work is dedicated to my family for their tremendous support and encouragement.

CHAPTER 1

INTRODUCTION

1.1 Brain tumors

Glioblastoma multiforme (GBM) is the most common and aggressive form of primary brain tumor in humans. Most of the malignant tumors originating in the brain are gliomas which arise from glial cells. Gliomas account for 40% of all primary brain tumors and 78% of malignant tumors (Fig. 1). Astrocytomas and glioblastomas account for 75% of all gliomas (Fig. 2). Although the most common site of involvement is the brain, gliomas can also affect the spinal cord, or any other part of the central nervous system (CNS), such as the optic nerves. Gliomas do not metastasize throughout the body, unlike most forms of cancer, but cause symptoms by invading the brain: if left untreated, the tumor is rapidly lethal.

Gliomas can be categorized according to their grade, which is determined by pathologic evaluation of the tumor: Low-grade gliomas are well differentiated, slower growing, biologically less aggressive, and portend a better prognosis for the patient. High-grade gliomas are undifferentiated or anaplastic, fast growing and can invade adjacent tissues, and carry a worse prognosis

There are numerous grading systems, but the most commonly used system is the World Health Organization (WHO) grading system for astrocytomas. The WHO system

assigns astrocytomas a grade from 1 to 4, with 1 being the least aggressive and 4 being the most aggressive. Various types of astrocytomas are given corresponding WHO grades. WHO Grade 1: e.g. pilocytic astrocytoma; WHO Grade 2: e.g. diffuse astrocytoma; WHO Grade 3: e.g. anaplastic (malignant) astrocytoma; WHO Grade 4: glioblastoma multiforme (most common glioma in adults).

Low grade (1 and 2) astrocytomas are typically benign, anaplastic astrocytomas (grade 3) normally progress from lower grade astrocytomas, and GBM is classified as grade 4 due to its high diffuse and invasive properties. GBMs are highly vascular and contain necrotic regions with pseudopalisading tumor cells, i.e., hypercellular zones surrounding foci of necrosis. The typical histological appearance of gliomas is illustrated in Fig. 3.

Symptoms of GBM depend on the area of the brain where the tumor evolves. Progressive weakness, speech and/or visual loss occur when "eloquent" brain regions are involved and often result in the detection of the tumor at its early stage of development. Tumors often become quite large before symptoms appear, causing increased pressure and headaches, seizures and in some cases, visual loss from swelling of the optic nerves.

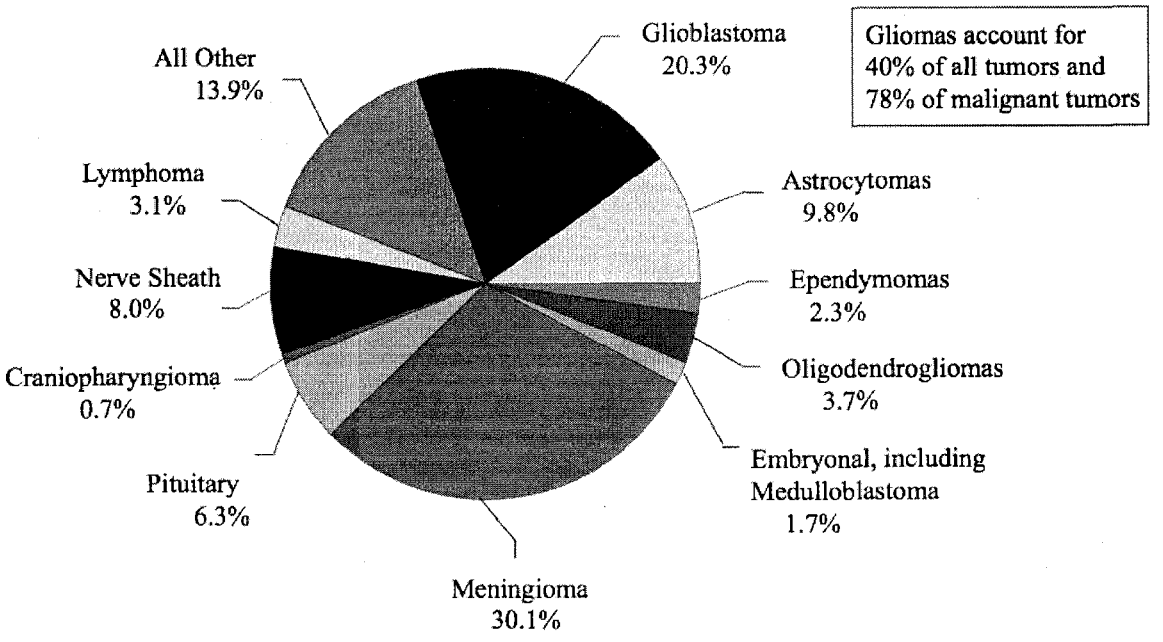

Figure 1. Distribution of primary brain tumors CBTRUS 1998-2002 (n=25,539). (CBTRUS Statistical Report, 2006)

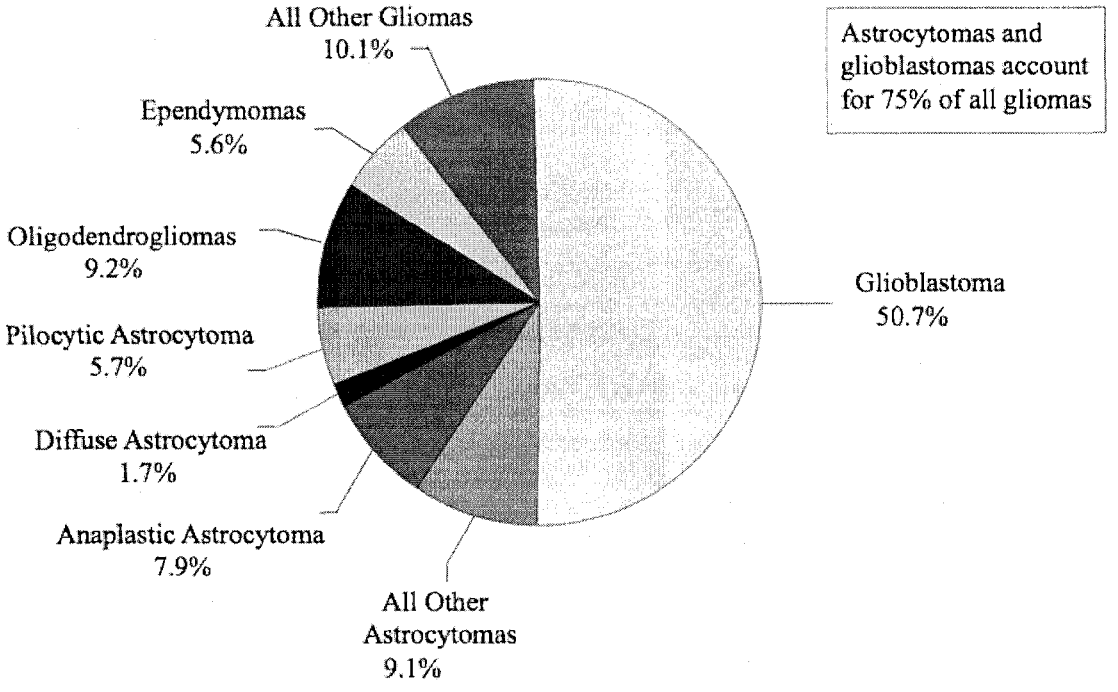

Figure 2. Distribution of gliomas by histology CBTRUS 1998-2002(n=63,698). (CBTRUS Statistical Report, 2006)

Progression	Normal Brain	Infiltrating Astrocytoma (WHO grade II)	Anaplastic Astrocytoma (WHO grade III)	Glioblastoma Multiforme (WHO grade IV)
Biology		Infiltration	Proliferation/expansion	Hypoxia/necrosis
Genetic events		p53 loss	p16, p14ARF loss PDGFR amplification	EGFR amplification chromosome 10 losses (PTEN)
Angiogenic events		VEGF ↑	PDGFR ↑ Angiogenesis	VEGF ↑↑ Microvascular hyperplasia

Figure 3. Glioma histology. Grade II individual tumor cells (black structures). In grade III anaplastic astrocytoma, cells become more numerous and atypical and are characterized by a high mitotic index. Glioblastoma multiforme (black arrows). Microvascular hyperplasia is often present as a glomeruloid vascular proliferation (white arrow). (Brat et al. 2002)

Once symptoms occur, the diagnosis of GBM is fairly straightforward. The tumor can be imaged by contrast-enhanced MRI. An open or needle biopsy provides tissue for microscopic diagnosis. Lower grade astrocytomas respond well to conventional therapies, while response of GBM to all current treatment modalities is very poor. The primary treatment for newly diagnosed GBM's is surgical resection (as enunciated in the National Comprehensive Cancer Network central nervous system guidelines) (Olson and Ryken 2008). Surgery is usually augmented by conventional fractionated external-beam radiotherapy to the tumor bed (as defined by the Radiation Therapy Oncology Group) (Harrison et al. 2003), and the administration of chemotherapeutic agents (e.g. the nitrosoureas such as BCNU, or more recently, temozolomide) (DeAngelis et al. 2001; Walker et al. 1978 and 1980; Byar et al. 1980; Yung et al. 2000; Sipos et al. 2002). There

are a number of treatment challenges associated with GBM: 1) location of tumors in eloquent areas of the brain preventing complete resection; 2) intrinsic resistance of lesions to conventional therapy; 3) limited capacity of the brain to repair itself; 4) the spread of malignant cells into the brain parenchyma; 5) the variably disrupted blood–brain barrier complicating drug delivery; 6) tumor capillary leakage with resultant peritumoral edema and intracranial hypertension; and 7) the neurotoxicity of treatments directed at gliomas.

The prognosis is worst for patients with Grade 4 gliomas or GBM. Despite recent advances in the therapy of patients with GBM, the median survival is still restricted to 12 months (Stummer et al. 2008). In recurrent disease, the best possible established second line-treatments, apart from surgery, are local chemotherapy with BCNU (Carmustine) wafers or temozolomide chemotherapy, which result in an overall survival of less than 8 months. Novel therapies, such as immunotoxins, administered via convection-enhanced delivery, or gene therapy have so far failed phase III evaluations. Therefore, new treatment options are desperately needed (Stummer et al. 2008).

Failure of treatment for high-grade gliomas, such as GBM, and its associated high mortality, is mostly due to the highly invasive nature of GBM cells, which leads to local recurrence at the site of surgical resection, namely in the 2- to 3-cm margin surrounding the resection cavity. A potential solution for improving the treatment outcome would be to increase the resection area, but in many instances this would be problematic due to drastic alterations in brain functionality. The failure of current treatment modalities results in poor survival which suggests that a more aggressive form of local therapy, such as PDT, could be of benefit.

1.2 Photodynamic therapy

PDT is a local form of therapy used as a treatment for a variety of cancerous and non-cancerous conditions. PDT involves administration of a tumor-localizing photosensitizer (light-sensitive drug), which can be activated by light of a specific wavelength. A light activated photosensitizer transfers energy to molecular oxygen creating singlet oxygen, which is a highly reactive and toxic species that rapidly reacts with cellular components causing oxidative damage, and ultimately leads to cell death.

Light therapy, both natural and artificial, has been used throughout history for healing purposes. Sunlight has been used for medical purposes since the time of the ancient Greeks; Hippocrates, the father of modern medicine, prescribed exposure to sunlight for a number of illnesses and conditions (e.g. acne). The presence of violet light (405 – 420 nm) in the solar spectrum has been found to activate a porphyrin (Coproporphyrin III) in Propionibacterium acne which damages and ultimately kills the bacteria by releasing singlet oxygen.

As the technique advanced, photodynamic therapy became increasingly widespread. Currently there are many clinics that use PDT for the treatment of various types of skin, lung, esophagus, prostate, eye, and brain tumors. PDT has a number of advantages over conventional treatment modalities (surgery, chemotherapy and radiation therapy) currently used in oncology. PDT is a highly localized form of treatment, and unlike chemotherapy or radiation therapy, which damage normal tissues, PDT causes little or no damage to normal tissue. Photosensitizers used for PDT of the brain have a relatively high tumor-to-normal brain selectivity (for some drugs this ratio is around 200:1 (Angell-Petersen et al. 2006)). By using optical fibers, light can be delivered locally to the tumor.

In biological systems, singlet oxygen generated by photochemical reactions has a very short half-life (< 40 ns) and therefore a short range of action (< 20 nm) (Moan et al. 1991) which minimizes damage to normal tissue. The probability of inducing secondary malignancies as a result of PDT is low, as most photosensitizers do not accumulate in cell nuclei and therefore PDT generally does not cause DNA damage, mutations and carcinogenesis unlike radiation therapy and some chemotherapeutic drugs.

The mechanisms by which photosensitizers selectively accumulate in tumors are complex and not fully understood. It is presumably due to abnormal tumor physiology which include decreased pH, high vascular permeability due to a leaky vasculature, lack of lymphatic drainage, increased number of low-density lipoprotein receptors and abnormal stromal composition. (Dougherty et al. 1998).

A number of in vitro and in vivo studies have been conducted to investigate the efficacy of PDT as an alternative therapy for high-grade gliomas. In vitro models, consisting of monolayer cell cultures, single cell suspensions, and multicellular spheroids, have been subjected to a wide variety of PDT treatment regimens. For example, PDT efficacy has been studied as a function of numerous parameters including photosensitizer dose and type, time of incubation, light dose and dose rate, and light fractionation schemes. Several animal glioma models have been developed for the study of PDT response in vivo. For example, F98 and BT4C rat glioma models have been used in a number of PDT studies since the resultant tumors mimic many of the chararacteristics (e.g. infiltrative and invasive behavior) of GBMs (Madsen et al. 2006 and Madsen et al. 2007). The results indicate that although PDT is capable of producing

significant tumor necrosis, the treatment often results in significant morbidity due to increased intracranial pressure caused by PDT-induced edema.

1.3 ALA - PDT

Typically, pre-synthesized sensitizers are used in PDT. The administration of the photosensitizer is followed by a delay period (from 30 min. to 7 days depending on the drug) to allow selective accumulation in tumor cells. Light irradiation occurs following the delay period resulting in either direct tumor cell kill, or indirect toxicity due to the destruction of the tumor vasculature. The use of precursor drugs, such as 5-aminolevulinic acid (ALA), constitutes a different approach to PDT since the drugs are converted to photosensitizers during intracellular biochemical processes.

ALA is a naturally occurring precursor in the biosynthetic pathway for heme production, as shown in Fig. 4. The last step in the biosynthetic route involves conversion of protoporphyrin IX (PplX), to heme. PpIX is a porphyrin-based photosensitizer which shows great promise in PDT. The compound is a planar aromatic molecule composed of four symmetrically arranged pyrrole subunits linked by four methane bridges (Fig. 5) (Gibson et al. 1999). Heme biosynthesis starts in the mitochondrion, and under physiologic conditions, cellular heme synthesis is regulated in a negative feedback control of the enzyme ALA synthase by free heme. ALA synthase then becomes the rate-limiting step. When exogenous ALA is added, the control mechanism is bypassed, and downstream metabolites are synthesized in excess. Under these conditions, ferrochelatase, which catalyzes iron insertion into PpIX, becomes the rate-limiting enzyme. Following the addition of exogenous ALA, the low physiologic rate of iron

insertion by ferrochelatase is unable to compensate for the excess PpIX that is formed. This leads to accumulation of PpIX in cells thus making them photosensitive. (Hasan et al. 2003; Bernigaud et al. 2008; Gibson et al. 1999) Shortly after administration of ALA (approximately four hours) significant amounts of PpIX accumulates in the mitochondria and cytosol. The type of cell death associated with ALA-PDT is sensitively dependent on the delay interval between administration and light irradiation. At short delay intervals, PpIX is largely confined to the mitochondrial membrane and light irradiation during this period results in mitochondrial membrane damage, which is associated with an apoptotic mode of cell death. At longer delay times, a substantial amount of PpIX may be found in the plasma membrane and resultant light irradiation will cause damage to this structure. Plasma membrane damage typically results in necrotic cell death.

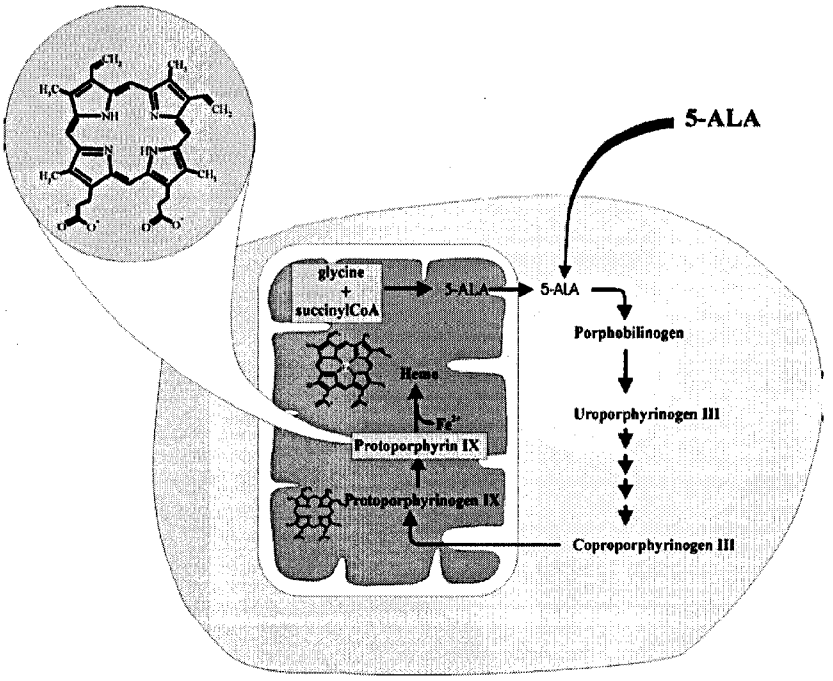

Figure 4. The heme biosynthesis pathway. ALA is converted to PpIX, the immediate precursor of heme. Heme regulates ALA synthase by negative feedback. Exogenous ALA administration bypasses this regulation and causes accumulation of PpIX. (Peng et al. 1997)

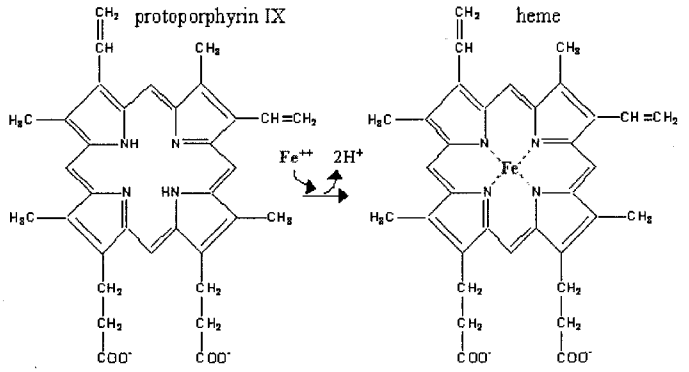

Figure 5. Protoporphyrin IX (left), is the immediate precursor of heme. Insertion of the iron atom into the ring structure of protoporphyrin IX generates heme (right).

As shown in Fig. 6, PpIX has a strong absorption peak at 635 nm. Combined with the relatively high penetration depth of 635 nm light in tissues, this provides the rationale for using this wavelength in ALA-PDT applications. The penetration depth of light is defined as the depth at which the light intensity decreases to 37% of its initial value. In normal brain and brain tumors, these depths are in the range of 1.5-3.0 mm for 635 nm light. (Angell-Petersen et al. 2006)

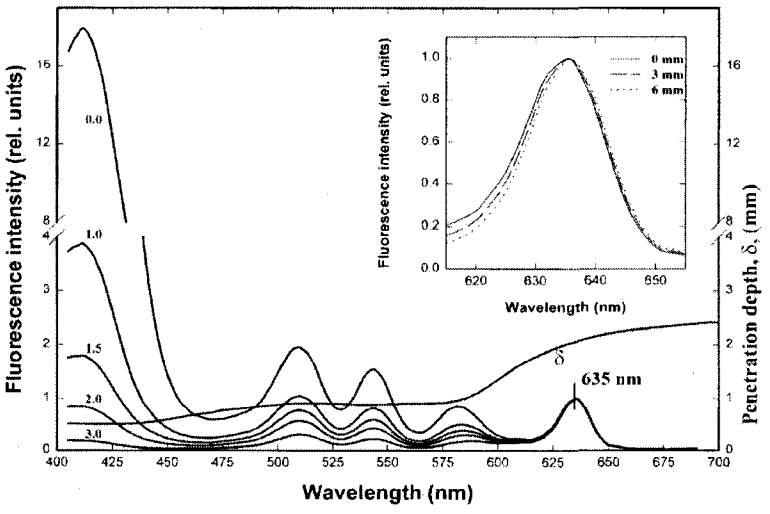

Figure 6. PpIX fluorescence excitation spectrum. The penetration depth (δ) of light in soft tissue increases with increasing wavelength. The expanded spectrum shows that PpIX fluorescence remains unchanged as a function of depth below the tissue surface (0 – 6 mm). (Peng et al. 1997)

1.4 Light and oxygen

The mechanism of action of PDT is summarized in Fig. 7. After administration, ALA accumulates in the mitochondria of tumor cells and enters the heme cycle. The end result of this process is the increased production of PpIX which, when exposed to 635 nm light results in its activation to an excited singlet state. Singlet PpIX then undergoes an intersystem crossing resulting in triplet PpIX which reacts with ground state triplet oxygen resulting in excited singlet oxygen – a highly reactive toxic species responsible for cell death.

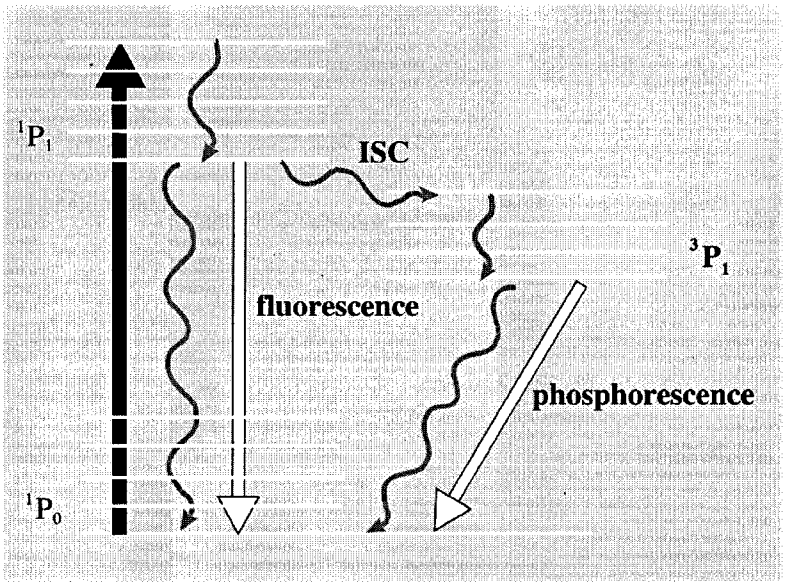

Figure 7. Jablonski diagram illustrating the interaction between PpIX and oxygen. The black arrow indicates the excitation of the photosensitizer to the excited singlet states ($^1P_1$). ISC - intersystem crossing; $^3P_1$ - the sensitizer in the triplet state. (Peng et al. 1997)

A diode laser is the most common light source for PDT, as it is compact, portable, and has a stable output, producing light of a fixed wavelength needed for photosensitizer activation. Light is typically delivered through an optical fiber which is directed to the treatment area. The efficacy of PDT is directly dependent on the production of singlet

oxygen, therefore tissues must be well oxygenated throughout the treatment. This may not always be the case as certain regions within the tumor may be hypoxic. Furthermore, PDT decreases oxygen levels in tissues by consuming oxygen during photodynamic reactions, and also by shutting down blood vessels. PDT efficacy may be severely compromised in situations where the rate of oxygen consumption exceeds the rate of reoxygenation. Potential solutions to this problem include the introduction of dark periods during treatment and the use of lower light fluence rates (Dougherty et al. 1998).

1.5 The blood-brain barrier and cerebral edema

The blood-brain barrier (BBB) is a membrane-like structure composed of tightly packed endothelial cells lining the internal walls of the brain capillaries (Fig. 8). Unlike peripheral endothelial cells, brain microvascular endothelial cells form a highly selective barrier that blocks penetration of most materials into the brain. The function of the BBB is to protect the brain and maintain homeostasis by restricting entrance of potentially harmful substances and by allowing the entrance of essential nutrients. Large or hydrophilic molecules are unable to cross the barrier by themselves without the use of specialized carrier-mediated transport mechanisms. The selective nature of the BBB is related to its structural components that include: continuous tight junctions, lack of fenestration and a low concentration of transport vesicles. Tight junction proteins block the paracellular space and restrict diffusion; they are continuous between adjacent endothelial cells lining the brain vasculature. Therefore, to reach the brain interior, molecules must pass through endothelial cells by transcytosis. Fenestrations are "holes" or "pores" (ranging from 60-350 nm in diameter) in regions of endothelial cytoplasm

through which materials can diffuse, enter or exit the cell. Endothelial vesicles carry solutes across endothelial cells, facilitating transport across blood vessels. Unlike peripheral tissues, where endothelial cells have many fenestrations and transport vesicles, endothelial cells lining the brain vasculature lack fenestration and have fewer transport vesicles. This significantly reduces passive diffusion across the brain endothelium and is the reason for the selective permeability of the BBB.

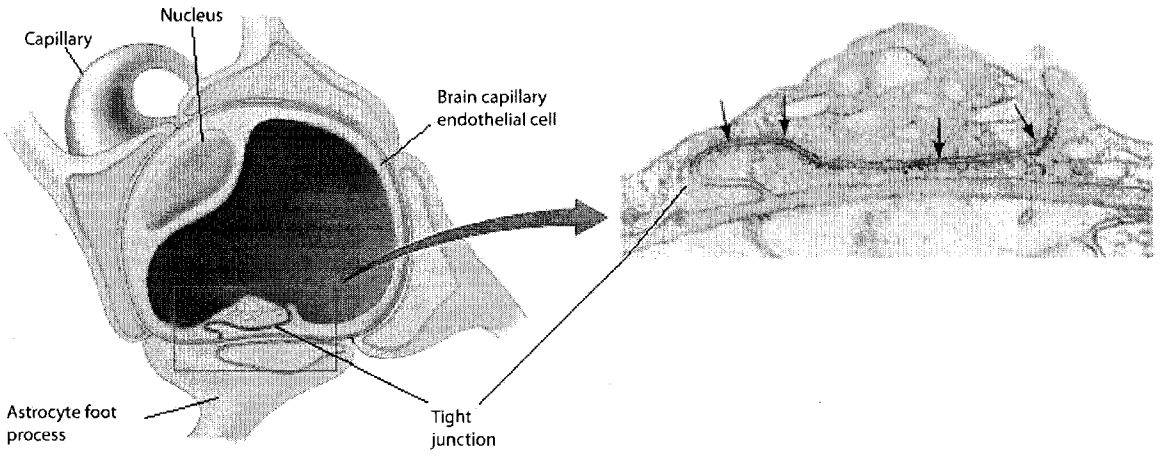

Figure 8. The blood brain barrier (BBB). Left: brain capillary in cross section showing the endothelial cell, tight junctions and the investment of the capillary by astrocytic end feet. The impermeability of the BBB mainly relies on the tight junction proteins between endothelial cells (Goldstein et al. 1986). Right: electron micrograph showing the appearance of tight junctions between neighboring endothelial cells (arrows). (Peters et al. 1991.)

Disruption of the BBB permits the entry of plasma fluid into the brain parenchyma, leading to cerebral edema formation. The word edema comes from the Greek word- οἴδημα which means "swelling"; it occurs as a result of the breakdown of tight endothelial junctions, which make up the BBB. Breakdown of this barrier allows normally excluded intravascular proteins and fluid to penetrate into the cerebral parenchymal extra-cellular spaces. Once plasma constituents cross the BBB, edema

spreads quite rapidly and may extend to large areas of the brain. As fluid enters white matter it moves extra-cellularly along fiber tracts and can also affect the grey matter. Cerebral edema may be either cytotoxic or vasogenic. Cytotoxic edema occurs due to changes in cellular metabolism resulting in inadequate functioning of the sodium-potassium pump in the glial cell membrane while the BBB remains intact. As is the case with other therapeutic interventions, it is assumed that PDT causes vasogenic cerebral edema, which occurs as a result of BBB degradation. The formation of cerebral edema is quite dangerous as it results in increased intracranial pressure, which impairs vascular perfusion and can lead to brain ischemia, herniation and death.

In pre-clinical studies, it has been shown that ALA-PDT is capable of causing significant brain tumor necrosis (Madsen et al. 2006). An unfortunate complication of this therapy is the induction of cerebral edema, which indicates that ALA-PDT damages endothelial cells constituting the BBB. The resultant increase in intracranial pressure produces significant morbidity and, in some cases, animals die soon after treatment (Madsen et al. 2006)). A potential solution to this problem is the administration of steroids, which have the potential to reduce ALA-PDT-induced endothelial cell swelling and concomitant re-establishment of the tight junctions responsible for BBB integrity.

1.6 Scope of study

The main purpose of this study is to understand the nature of ALA-PDT-induced cerebral edema formation caused by localized disruption of the BBB. Detailed knowledge of the parameters affecting edema formation is required in order to optimize ALA-PDT for patients with high-grade gliomas. It is hypothesized that: (1) the extent of ALA-PDT-

induced edema in normal rat brain is dependent on light fluence – higher fluences will produce larger edema volumes; (2) the extent of edema will peak approximately 1-2 days following PDT and thereafter, will diminish rapidly and (3) edema volumes will be smaller in animals treated with steroids.

CHAPTER 2

MATERIALS AND METHODS

2.1 Animal care

Inbred male Fischer 344 rats (Simonsen Laboratories, Inc, Gilroy, CA) weighing at least 300 g were caged in Macrolon III cages. The animal holding rooms were maintained at constant temperature and humidity on a 12-hour light and dark schedule at an air exchange rate of 18 changes per hour. Animal care and protocol were in accordance with institutional guidelines. For the surgical procedures, the rats were anaesthetized with pentobarbital (25 mg/kg i.p.). Buprenorphin (0.08 mg/kg s.c.) was used as a post-operative analgesic. The animals received a total of seven doses administered at 12 h intervals. All animals were euthanized with Pentobarbital (100 mg/kg i.p.) at the first signs of distress.

2.2 ALA-PDT in Fischer rats

Tumor-free rats were used in all studies. The different PDT treatment protocols examined are summarized in Table 2.1. Briefly, the extent and time evolution of ALA-PDT-induced cerebral edema was evaluated in five groups of animals subjected to varying light fluence and steroid conditions.

Table 2.1. Experimental groups

Group	Description	n	Purpose
1	Normal brain + 5-ALA-PDT (26J, 10mW)	9	Study the extent of edema in normal brain in response to 5-ALA-PDT
2	Normal brain + 5-ALA-PDT (17J, 10mW)	7	Study the extent of edema in normal brain in response to 5-ALA-PDT
3	Normal brain + 5-ALA-PDT (9J, 10mW)	4	Study the extent of edema in normal brain in response to 5-ALA-PDT
4	Normal brain + 5-ALA-PDT (17J, 10mW) + Steroids	4	Determine effects of steroids on 5-ALA-PDT induced edema in normal brain
5	Normal brain + Light (No ALA) Control Group	4	Rule out the possibility of hyperthermia- induced edema

Four to five hours prior to light treatment, animals were injected with 125 mg/kg ALA intraperitoneally (i.p.). Before treatment, animals were anesthetized, fixed in a stereotactic frame (David Kopf Instruments, Tujunga, CA) and the skin covering the skull was incised. A 1.0-mm burr hole was then made with an 18-gauge needle. A 400-μm bare flat-end quartz fiber with numerical aperture of 0.22 was introduced directly into the brain according to the following coordinates: 3 mm posterior to and 2 mm to the right of the bregma with a depth of 5 mm below the dura. Light from a 635 nm diode laser was delivered interstitially (10 mW fluence rate) for a total light fluence of 26 (group 1), 17 (group 2) or 9 J (group 3). The corresponding treatment times were 43, 28 and 15 minutes, respectively. In all cases, moisturizing gel was applied to the animal's eyes and the rat was wrapped in a towel to prevent hypothermia. At the conclusion of treatment, the fiber was withdrawn from the brain, and the burr hole was sealed with bone wax. The

fourth group of animals was subjected to ALA-PDT (26 J, 10 mW) as described above and treated with steroids in order to gauge their effects on edema formation. Steroids (Solu-Medrol – 1 mg/kg per fraction) were administered in 4 fractions: 1 day prior to PDT, on the day of PDT and on 2 consectutive days following PDT. Animals in the control group (group 5) were subjected to light treatments (26 J at 10 mW) in the absence of photosensitizer to rule out the possibility of hyperthermia-induced edema.

2.3 Magnetic resonance imaging

High-field (3 T) magnetic resonance imaging (MRI) was used for screening and detecting the extent and time evolution of PDT-induced edema in the brains of Fischer rats. This imaging technique is ideally suited for evaluating the extent and time course of edema formation and its noninvasive nature minimizes the number of animals required for the studies.

Due to its high water content, edema appears hyperintense (bright) on T2-weighted (T2w) images and hypointense (dark) on T1-weighted (T1w) images. Contrast agents were administered to determine BBB disruption. The appearance of contrast enhancement on T1w images following contrast administration was suggestive of BBB disruption.

All animals were subjected to the same scanning procedure. Rats were transported to the imaging facility via climate controlled private vehicle. Prior to scanning, animals were anesthetized with Pentobarbital as previously described. All scanning was performed after hours to avoid patient contact. A high field (3 T) MRI (Philips Medical Systems, Bothell, WA) scanner was used to acquire all images using the acquisition

parameters listed in Table 2.2. The anesthetized animal was placed in a specially designed lucite immobilization device, which was inserted into the scanner and T1w and T2w images were acquired (Fig. 9).

Table 2.2. MRI acquisition parameters

Acquisition	TR (ms)	TE (ms)	Flip angle	FOV (mm)	Slice thickens (mm)	Slice gap (mm)	Number of slices	Matrix size
T1W	495	10	85°	40 × 40	1.5	0	20	80
T2W	3418	80	90°	40 × 40	1.5	0	20	80

Images were obtained using a flexible surface coil (normally used for scanning the human shoulder), which was positioned around the immobilization device. Following the initial T1 and T2 imaging sequences, the animal was removed from the scanner and injected (i.p.) with a commercial gadolinium-based contrast agent (1.0 ml of 0.5 mmol/ml Magnevist: Berlex Laboratories, Wayne, NJ). Approximately 15 min post injection, animals were rescanned using a T1w pulse sequence. The total acquisition time for the three scans (T1-pre, post and T2-pre) was approximately 15 min. Following the image procedure, each animal was placed in its cage and transported back to UNLV's Animal Facility. All animals were scanned 4 times, on the day after PDT (day1), and on days 3, 7 and 14.

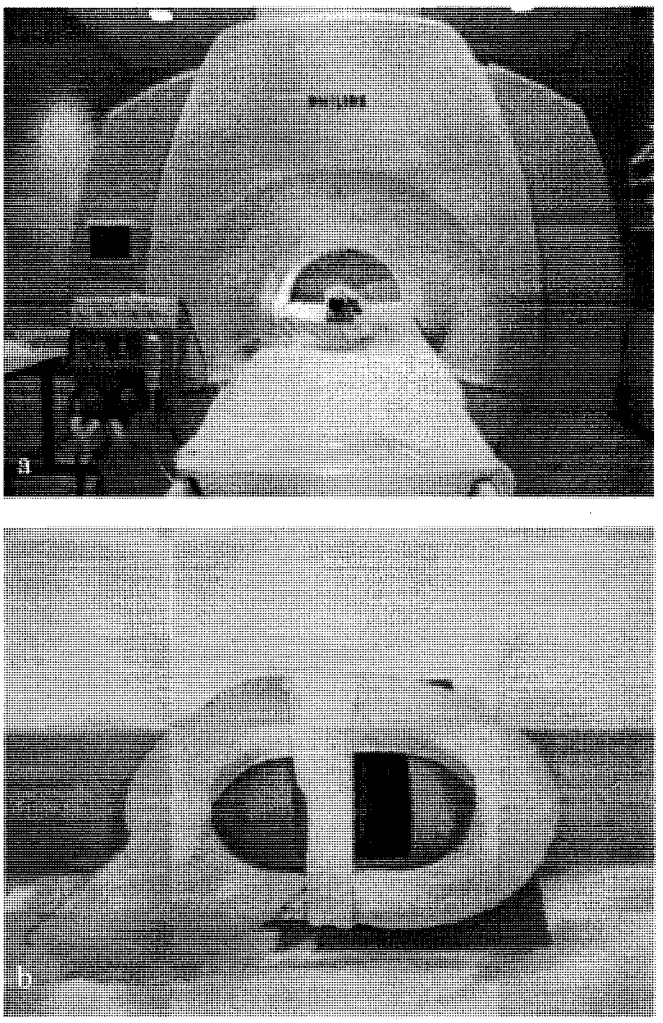

Figure 9. Imaging setup. a: the high field human MR scanner, b: animal in the immobilization device surrounded by a surface coil.

2.4 Histological preparation

Animals were sacrificed 15-17 days following PDT treatment and their brains extracted. The brains were sectioned along the fiber injection track and fixed by immersion in 10 % buffered (pH 7.2) formalin prior to paraffin embedding. Four micrometer thick coronal sections were obtained from the original cut surface representing the position of the fiber track and thereafter at 1, 2 and 3 mm depths. The sections were stained with hematoxylin and eosin (H&E) and examined under a light microscope by an independent pathologist blinded to the treatment modes.

2.5 Image analysis

Data was analyzed using OsiriXVP software (Fig. 10). Hyperintense signal regions (excluding CSF) on the T2w MRI images represent edema. Areas of suspected edema content were manually outlined on each slice.

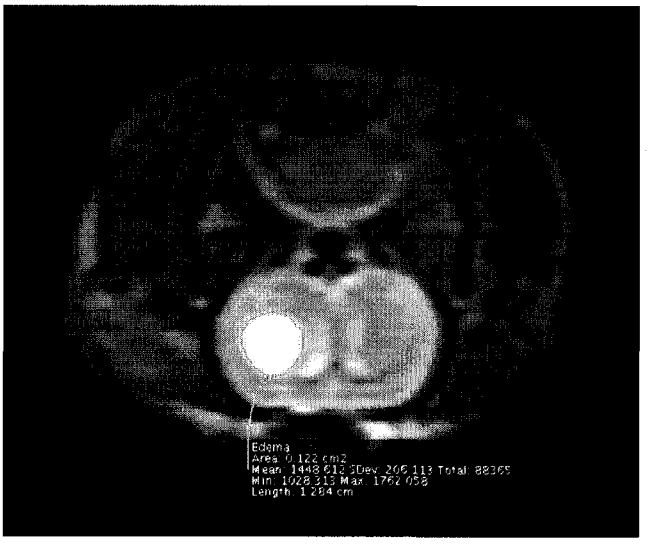

Figure 10. Image analysis. Hyperintense signal regions on the T2w image represent cerebral edema. Contouring was performed manually, and edema volume determined using OsiriXVP software.

Edema volume was calculated according to the following equation:

$$V=\sum(S_i \cdot 0.15)\ cm^3$$

Where S_i represents the area of the contoured region on slice i as determined by the OsiriXVP software, and 0.15 is the slice thickness in cm.

CHAPTER 3

RESULTS

3.1 Light fluence

As shown in Figs. 11 and 12, edema formation was sensitively dependent on the PDT light fluence: Increased light fluences (9, 17 and 26 J) resulted in a fluence-dependent increase in post-operative edema.

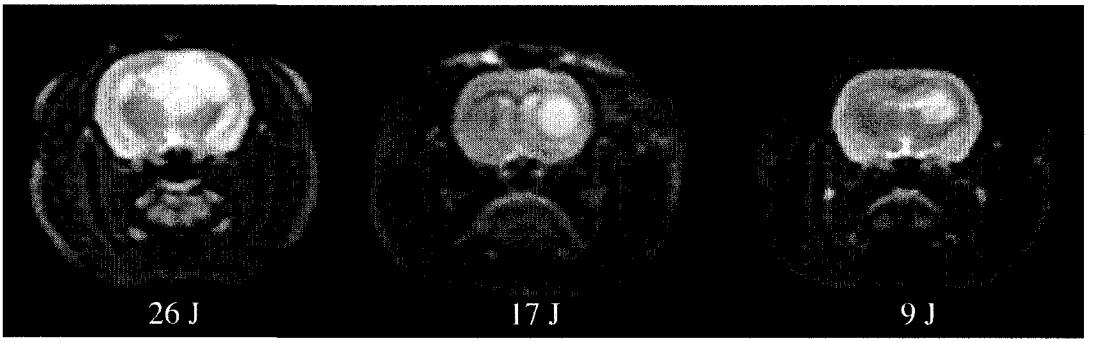

Figure 11. T2w MR images illustrating the dose dependence of edema formation. In all cases, light was delivered at a fluence rate of 10 mW and images were acquired 1 day following PDT.

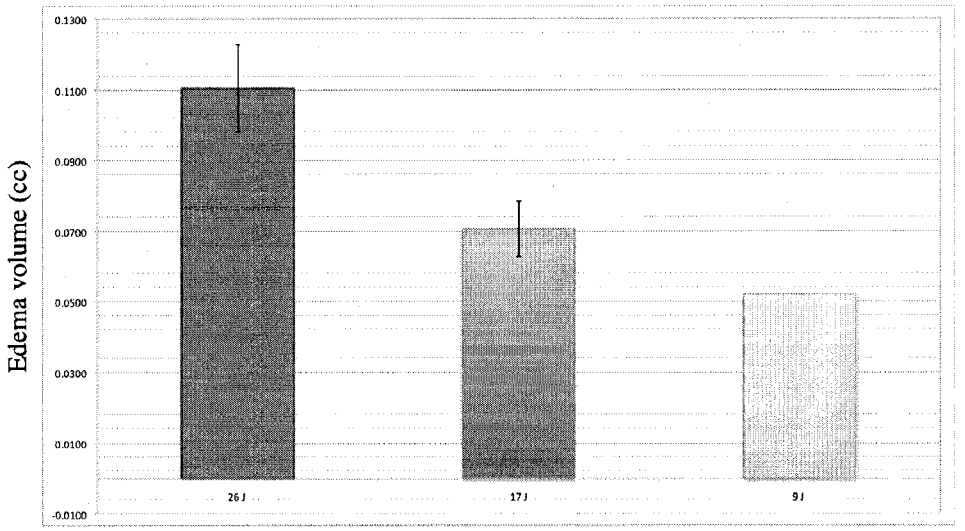

Figure 12. Edema volume as a function of light fluence 1 day post-PDT treatment.

3.2 Histological analysis

In areas exposed to the highest fluence levels (5-15 μm from the fiber), no significant pathology was observed in coronal sections obtained from animals subjected to a fluence of 9 J (Fig. 13c). At higher fluence levels of 17 J, extensive infiltration of lymphocytes and macrophages (some loaded with hemosiderin) was apparent (Fig. 13d). Blood vessels in these sections showed hyperplastic endothelial cells. At fluence levels of 26 J (data not shown), a focally extensive area of necrosis with some degeneration of brain parenchyma and infiltration of lymphocytes, plasma cells and foamy macrophages (Gitter cells) was apparent in the immediate area of the fiber tip. Some of the Gitter cells contained hemosiderin, which is suggestive of treatment-induced hemorrhage. Blood vessels in these sections also showed hyperplastic endothelium. In contrast, sections taken 1, 2 or 3 mm from the fiber track showed no significant pathology for all three of the fluence levels tested. Histological sections taken from the brains of light-only control animals showed no pathology (data not shown).

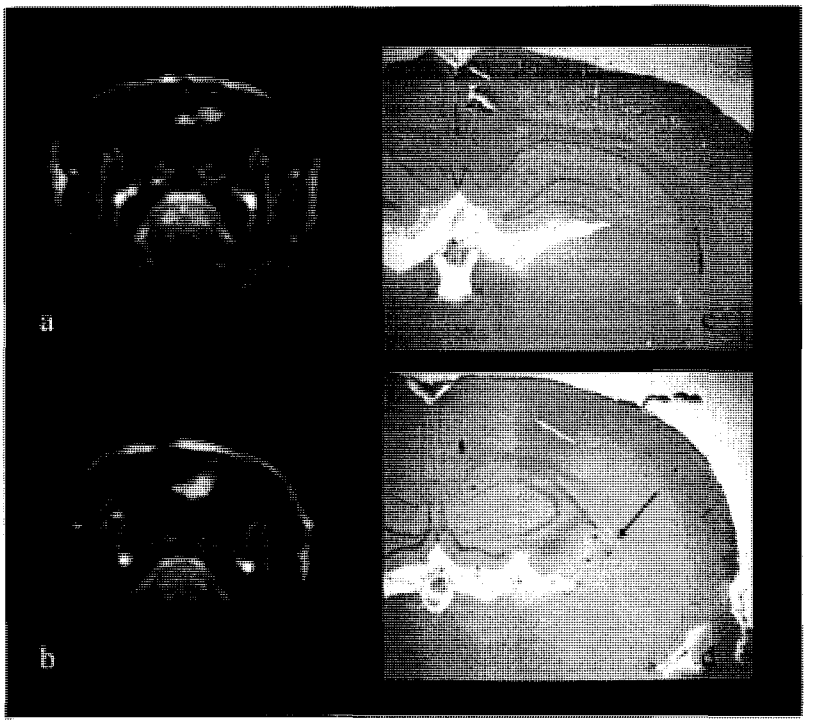

Figure 13. T1w MRI contrast enhanced images (a, b) showing focal contrast enhancement centered around the area of light treatment. PDT treatment to a fluence level of 9 (a) and 17 J (b), at a fluence rate of 10 mW was performed 4 h following ALA administration (125 mg/kg i.p.). Both scans were performed 1 day post PDT and 15 minutes following i.p. contrast injection. (c, d) Coronal H&E sections from the brains of animals corresponding to a and b taken 15 days post treatment. In the area exposed to the highest fluence level (5-15 μm from the fiber) no significant pathology was observed following delivery of 9 J (c). At a fluence level of 17 J, extensive infiltration of lymphocytes and macrophages (some loaded with hemosiderin) was apparent as denoted by the arrow in (d).

3.3 Time evolution of edema

Analyses of T2w images show a marked decrease in edema volume as a function of time post-PDT treatment (Figs. 14 - 16). At the highest fluence investigated (26 J), edema volume decreased by approximately 50% within a three-day time period post-treatment. This time period was found to be a significant prognostic indicator since any animal alive on day three was found to be a long-term survivor. Among surviving animals, the edema

was almost completely resolved by day 14. The results presented in Fig. 16, suggest a simple exponential decrease in edema volume with time post- treatment.

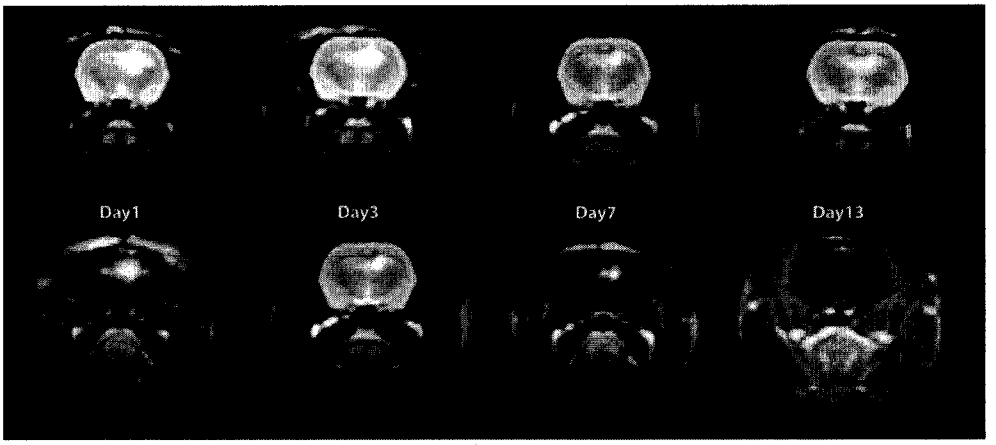

Figure 14. Time course of edema development (upper panel: T2w images) and contrast enhancement (lower panel: T1w post-contrast images). Light fluence and fluence rates were 26 J and 10 mW, respectively.

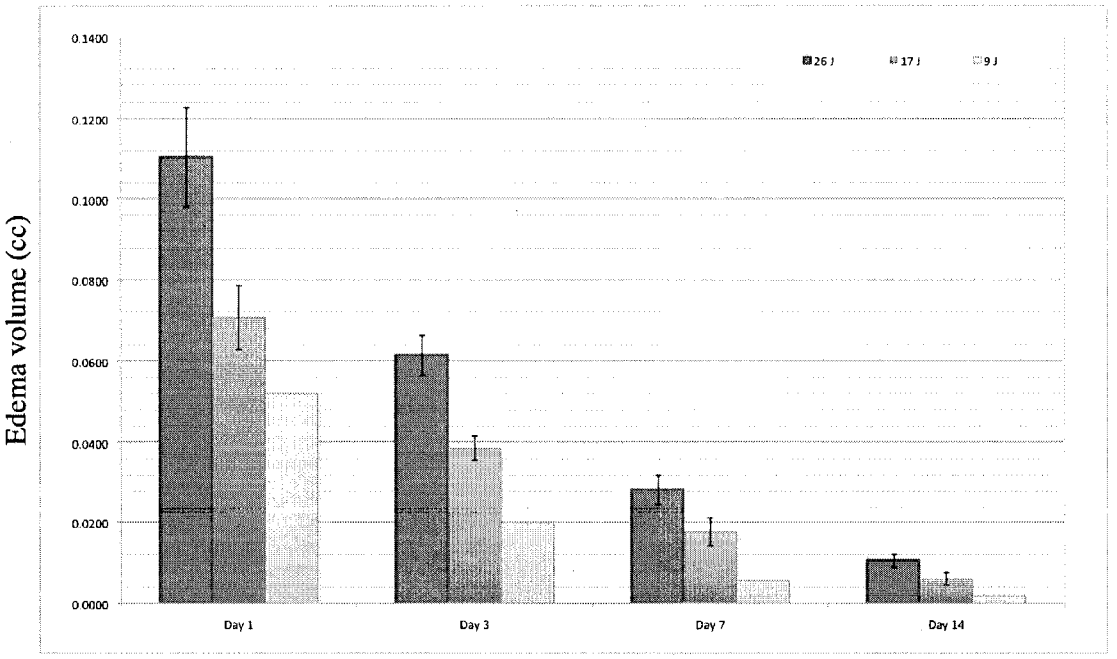

Figure 15. Time course of edema development in animals treated with 26, 17 and 9 J. In all cases, light was delivered at a fluence rate of 10 mW.

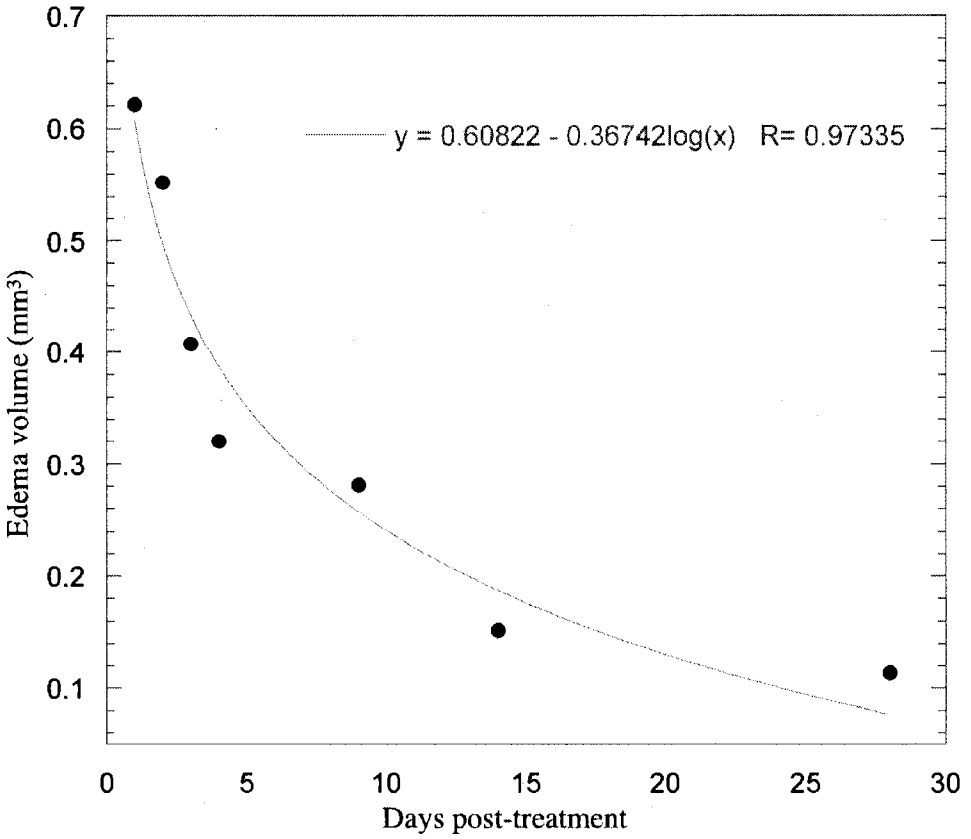

Figure 16. Decrease in edema volume as a function of time in PDT- treated animals. Light fluence and fluence rates were 17 J and 10 mW, respectively. The curve represents the best exponential fit to the data.

3.4 Blood-brain barrier patency

Post-contrast T1w images are illustrated in Fig. 17. Contrast volumes were measured on T1w images as a function of time post-contrast administration (Fig. 18). The results in Fig. 18 show a significant diminution in contrast volume as a function of days post-treatment (day 1 – day 17). The data also show that the rate of increase in contrast volume decreases with increasing time post-treatment. Taken together, the results suggest that the BBB is closing over the 17-day observation period.

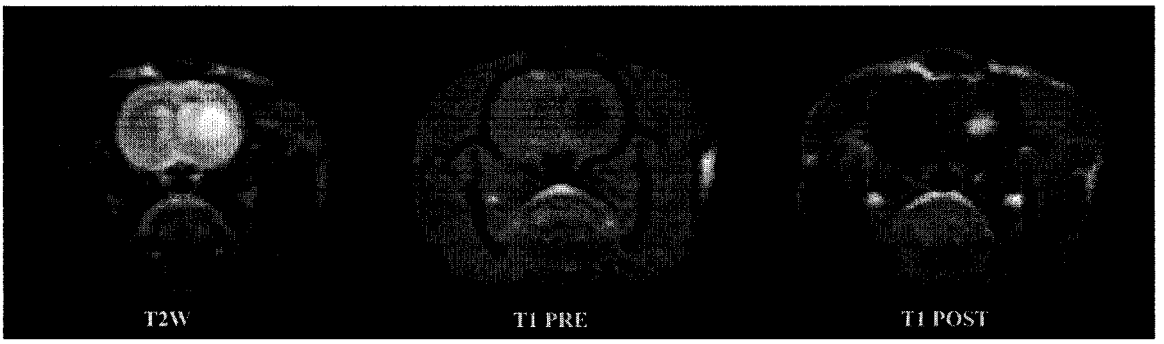

Figure 17. T2w, T1w-pre and -post contrast enhanced MRI images acquired 1 day following PDT. Due to its high water content, edema appears hyperintense (bright) on T2w images and hypointense (dark) on T1w images. Contrast agents were administered 15 min. prior to scans in order to determine BBB disruption. The appearance of enhancement on T1w images following contrast administration suggests BBB disruption.

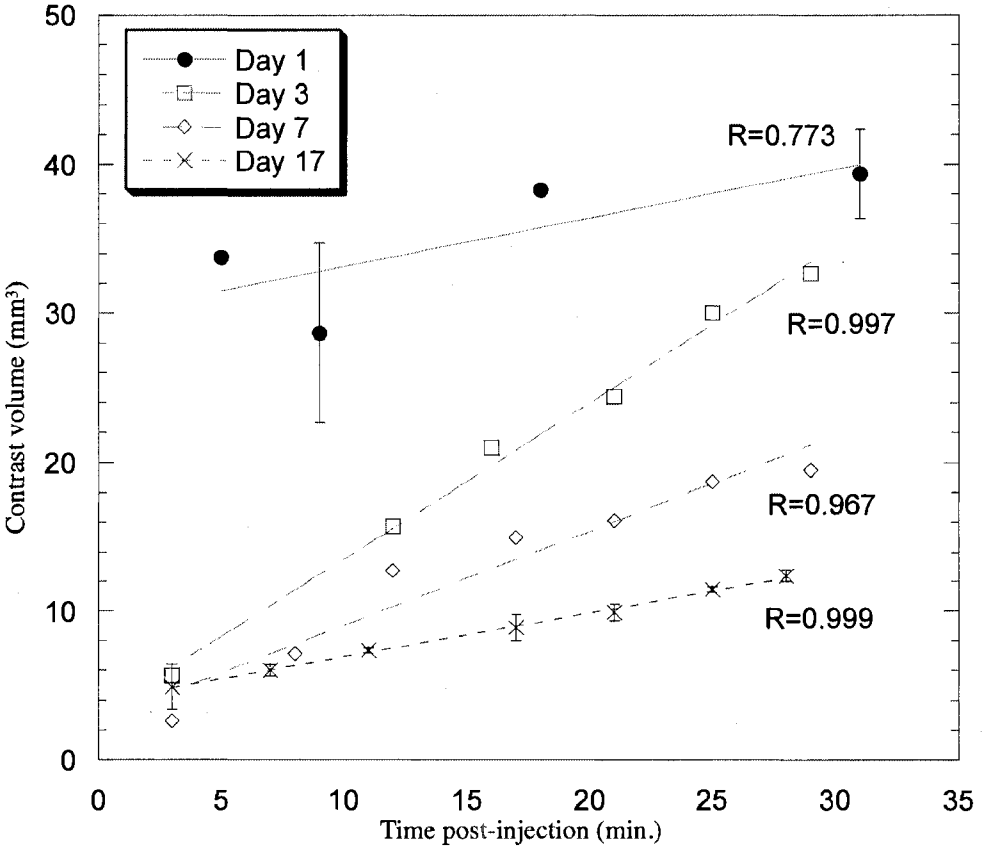

Figure 18. Contrast flow rate across the compromised BBB as a function of time post-contrast injection and time post-treatment. Light fluence and fluence rates were 9 J and 10 mW, respectively.

3.5 ALA - PDT + steroid treatment

Steroid treatment resulted in an anticipated reduction of post treatment PDT-induced edema formation. Animals treated with steroids, showed immeasurably small or no edema on pre-contrast T2 MR images (Fig. 19).

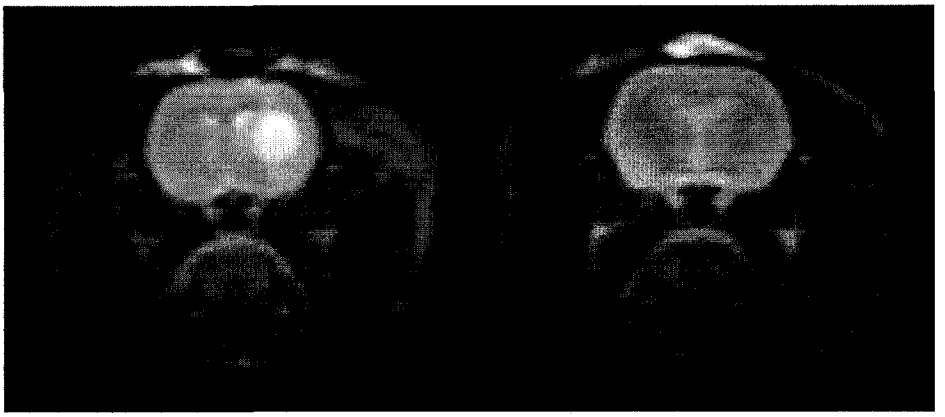

Figure 19. T2w MRI scans of normal rat brains. Left: animal subjected to ALA - PDT developed edema. Right: animal treated with ALA - PDT and steroids (Solu-Medrol - 1 mg/kg per fraction; total of 4 fractions). Both groups of animals received 125 mg/kg ALA ip 4 hours prior to light treatment. All animals were treated with 17 J light at a fluence rate of 10mW. Both animals were imaged 1 day following PDT.

3.6 Controls

As illustrated in Fig. 20, irradiation with laser light alone (26 J, 10 mW) without ALA administration provoked no visible damage in the brain tissue. Furthermore, animals did not show any abnormal behavior or signs of distress typical for the presence of intracranial edema.

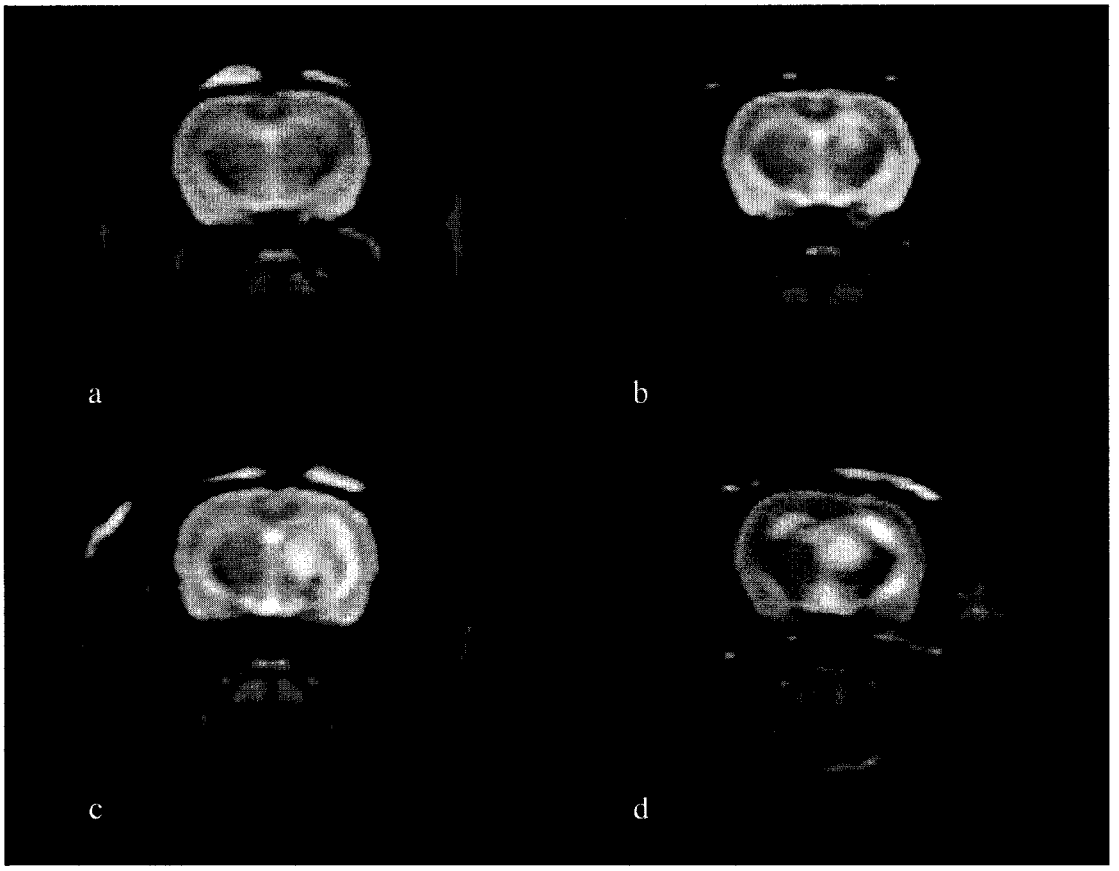

Figure 20. T2w MRI scans of rat brains. ALA vs no ALA. a: Light only 26J, b: 9 J, c: 17 J, d: 26 J. b, c, d, received 125 mg/kg ALA ip 4 hours prior to light treatment (10mW). Images were acquired two days following light treatment.

CHAPTER 4

DISCUSSION

Despite ongoing research, the prognosis for patients suffering malignant gliomas remains poor with a median survival time of one year for GBM and three years for anaplastic astrocytoma (Chang et al. 1998). Following surgery, tumors recur locally in more than 80% of cases (Bashir et al. 1988; Wallner et al. 1989). This would suggest that a more aggressive form of local therapy, such as PDT, might delay the onset of tumor recurrence and hence result in prolonged survival.

A number of rat brain tumor models have been used to investigate the efficacy of PDT for the treatment of malignant gliomas. Although several studies have shown that PDT is capable of producing significant tumor necrosis, associated edema often results in severe morbidity and mortality (Madsen et al. 2006; Ito et al. 2005). The primary objective of the present work was to evaluate the extent of ALA-PDT-induced cerebral edema in normal rat brain.

The results presented in this work clearly show that ALA-PDT is capable of disrupting the BBB resulting in light fluence-dependent cerebral edema. As illustrated in Figs. 11, 12 and 15, higher light fluences produced greater edema volumes. Of particular interest are the results showing that the edema dissipates over time (Fig.s 14, 15, 17) suggesting that BBB disruption is reversible and that complete restoration of the BBB is

possible, although this is clearly a light fluence-dependent phenomenon. Histological analyses (Fig. 13) revealed that damage to the BBB occurs following exposure to relatively low light fluences: extensive damage was observed at 17 J while no residual damage was evident at 9 J suggesting a damage threshold somewhere between these light fluences. The substantial edema volumes observed following high fluence PDT (26 J) was attributed to more extensive BBB damage. Not surprisingly, a significant number of animals in this group (29 %), died shortly after treatment due to their large edema burden. Day 3 of the post-PDT period appeared to be critical: animals that survived past this point made a full recovery. This is hardly surprising given the precipitous drop in edema volumes between days 1 and 3 (Fig. 15). Interestingly, edema volumes were observed to decrease exponentially following PDT (Fig. 16).

BBB dynamics can be inferred from the contrast flow rates presented in Fig. 18. The data show that contrast flow rates decreased sharply over the 17 day observation period suggesting that the BBB is closing during this interval. The mechanisms by which PDT leads to BBB degradation are not clear but likely include direct PDT effects on the endothelial cytoskeleton that lead to cell rounding and contraction, probably mediated by PDT-induced microtubule depolarization (Sporn and Forter 1992). In addition the formation and/or enlargement of endothelial gaps, has been observed in response to PDT (Fingar 1996). Additional evidence from fluorescence microscopy studies (Angell-Petersen et al. 2006) showing trace amounts of ALA-induced PpIX in presumptive normal brain support the hypothesis that a direct effect on the capillary endothelial cells is the most probable cause for the BBB degradation.

Low fluence rate/low fluence PDT has been demonstrated to enhance the delivery of macromolecular drug carriers, in particular liposomally encapsulated doxorubicin (Doxil) into murine colon carcinoma tumors growing in the shoulders of mice (Snyder et al. 2003) These results are in good agreement with other studies which have found a significant increase in edema formation, in orthotopic brain tumors, following ALA-mediated PDT in a rat brain tumor model indicating a breakdown of the blood-tumor barrier (BTB) (Angell-Petersen et al. 2006; Hirschberg et al. 2007). In these cases, the BTB was significantly altered by PDT most probably in a similar manner to the one proposed here for the BBB by enlarging endothelial gaps. In a recent paper, Hu et al. (2007), using a rat C6 glioma model and electron microscopy, showed that PDT changed the sub-cellular structure of the BTB with a reduction in the number of cellular components in endothelial cells of the capillary blood vessels. They also observed stretching of the tight junctions, with an enlargement of the gaps between endothelial cells and, in addition, PDT was found to have only a minimal impact on the normal sub-cellular structures of the BBB suggesting that the endothelial cells comprising the BBB were not permanently damaged by the treatment. These observations are in good agreement with the findings of this study, which showed that low fluence PDT was capable of inducing BBB disruption, as evidenced by contrast enhancement on MR images, yet no permanent damage was found in histological sections (Fig. 13c). In contrast, high fluence levels are clearly capable of causing significant tissue damage (Fig. 13d). For example, the tissue damage and immune cell infiltration observed in the region in close proximity to the light source are consistent with cerebral ischemia resulting in a localized stroke.

The use of steroids for the management of treatment-induced edema is a common strategy employed in the clinic. As shown in Fig. 19, the use of steroids resulted in a dramatic decrease in PDT-induced edema and therefore represents a good strategy for reducing morbidity and mortality in rats following PDT.

Steroids are powerful immunosuppressive and anti-inflammatory agents which mediate BBB dynamics. The exact mechanisms of action are not entirely understood and are the subject of intense study. Solu-Medrol (methylprednisolone sodium succinate) – a synthetic glucocorticoid drug was used in this study. Glucocorticosteroids (GCSs) act by binding to the intracellular glucocorticoid receptor, resulting in up-regulation or down-regulation of specific genes that encode proteins responsible for several cytokines and adhesion molecules (Singhal 2006).

The key factors that regulate the permeability of the BBB are vascular endothelial growth factor (VEGF), angiopoietin-1 (Ang-1), and angiopoietin-2 (Ang-2) (Kaal et al. 2004; Lee et al. 2003; Hori et al. 2004; Nag et al. 2005). VEGF is a key regulator of angiogenesis and was initially identified as a vascular permeability factor owing to its potent property of increasing the permeability of the vascular wall (Senger et al. 1983). VEGF disrupts junctions between endothelial cells, leading to increased vascular permeability, which results in the breakdown of the BBB (Weis et al. 2005). Angiopoietins are ligands for Tie-2, which is a receptor tyrosine kinase expressed on endothelial cells and hematopoietic stem cells (Dumont et al. 1992; Iwama et al. 1993). Among angiopoietins, the best characterized are Ang-1 and Ang-2 (Yancopoulos et al. 2002). Ang-1 induces autophosphorylation of Tie-2, while Ang-2 acts as a natural antagonist in endothelial cells in the presence of Ang-1 (Maisonpierre et al. 1997). Ang-1

precludes blood vessels from leaking while Ang-2 destabilizes the vessels. Ang-1 secreted by brain astrocytes and pericytes contributes to formation of the BBB (Lee et al. 2003; Hori et al. 2004), whereas Ang-2 directly results in breakdown of the BBB (Nag et al. 2005).

It has been suggested that additional nongenomic pathways exist for steroid effects occurring at higher concentrations (Singhal 2006). These result from action on membrane-bound receptors (specific nongenomic effects) or via physicochemical interactions with cellular membranes (nonspecific nongenomic effects). The nongenomic effects accelerate the termination of inflammation and may provide the molecular basis for the use of high-dose corticosteroids given during pulse therapy. GCSs regulate the expression levels of three key factors regulating the BBB: VEGF, Ang-1, and Ang-2 in BBB-comprising cells such as human brain astrocytes (HBAs), human brain pericytes (HBPs), and human brain microvascular endothelial cells (HBMECs). GCSs up-regulate Ang-1 and down-regulate VEGF in HBAs and HBPs, suggesting a novel mechanism for steroid-mediated stabilization of the BBB.

The results of the present study demonstrate that low light fluence ALA-PDT results in transient edema suggesting localized opening of the BBB in a reversible manner. It thus appears that PDT could offer an alternative to other strategies that have been developed to circumvent the BBB including the development of lipid soluble drugs, or the use of water-soluble agents with high affinities for natural carriers at the BBB (Pardridge et al. 2002; Pardridge et al. 2002). Present techniques for opening the BBB, including intra-arterial mannitol infusions, are problematic since they result in widespread opening of the BBB allowing entry of cytotoxic drugs and other circulating

molecules to both the tumor and normal brain in equal quantities (Doolittle et al. 2000). For a drug delivery system to be successful, transient and localized targeting of the BBB is required. PDT applied through an indwelling balloon applicator, filling the resection cavity, could satisfy this requirement (Madsen et al. 2001).

CHAPTER 5

CONCLUSIONS

MR imaging proved to be a highly effective and non-invasive method for following the development of edema formation and the degree and time course of BBB disruption, thus allowing the use of fewer animals. The MR images acquired in this study clearly showed that ALA-PDT caused local disruption of the BBB resulting in edema in normal rat brain. The extent of PDT-induced edema was dependent on light fluence: higher fluences resulted in increased edema volumes. Only small amounts of edema were observed at the smallest fluence investigated (9 J) whereas extensive edema and associated morbidity resulted following exposure to the highest fluence (26 J). Histological studies showed that light fluences as low as 17 J were capable of producing long-lasting damage in the rat brain. No permanent damage was observed following exposure to 9 J.

Although the exact dynamics of edema formation is somewhat difficult to determine from this study, the data suggest that edema volumes peaked approximately 24 h following ALA-PDT. Thereafter, edema volumes dissipated rapidly, and in an exponential manner, suggesting that BBB disruption was reversible and that complete restoration of the barrier was possible, at least at the lower light fluences. This is an important observation since it suggests that low light fluence PDT may be used in

therapeutic approaches to cause selective and transient opening of the BBB thus facilitating the delivery of anti-cancer agents to infiltrating glioma cells normally protected by the barrier.

Steroid treatment was found to be very effective at reducing PDT-induced edema and represents a sound strategy for reducing morbidity following high light fluence PDT. The aim of future studies will be to optimize steroid treatment regimens, including doses and fractionation schemes, in order to minimize PDT-associated edema. Additional studies should also be undertaken in order to gain a better understanding of the effects of light fluence on the extent of BBB disruption. For example, electron microscopy is ideally suited for determining the size of PDT-induced opening of the barrier. Alternatively, MR spectroscopy could be used to assay for the presence of large proteins (exogenous or endogenous) normally excluded from the brain by the intact BBB. In this scheme, the size of the BBB opening can be inferred from the protein size.

In conclusion, the extent of edema formation in response to ALA-PDT was found to be sensitively dependent on the light fluence. The high light fluences often used in the treatment of animal brain tumors resulted in widespread edema and severe morbidity. In contrast, the lowest light fluence (9 J) investigated in this work produced only a small amount of edema and therefore it would appear that low light fluence ALA-PDT may be a reasonable approach for targeted drug delivery to the brain. This has implications for the treatment of a variety of CNS diseases including gliomas.

REFERENCES

Angell-Petersen E, Madsen SJ, Spetalen S, Sun C-H, Peng Q, Carper SW, Hirschberg H. Influence of light fluence rate on the effects of photodynamic therapy in an orthotopic rat glioma model. J Neurosurg. 104(1):109-17; 2006.

Bashir R, Hochberg F, Oot R. Regrowth patterns of glioblastoma multiforme relating to the planning of interstitial brachytherapy. Neurosurgery 23: 27–30; 1988.

Bernigaud V, Drenck K, Huber BA, Hvelplund P, Jabot T, Kadhane U, Kirketerp MB, Liu B, Lykkegaard MK, Manil B, Nielsen SB. Electron-Capture-Induced Dissociation of Protoporphyrin IX Ions. J Am Soc Mass Spectrom; 2008.

Betz AL, Coester HC. Effect of steroids on edema and sodium uptake of the brain during focal ischemia in rats, Stroke 21, 1199–1204; 1990.

Brat DJ, Castellano-Sanchez A, Kaur B and Van Meir E.G. Genetic and biologic progression in astrocytomas and their relation to angiogenic dysregulation. Adv. Anat. Pathol. 9, 24-36; 2002.

CBTRUS Statistical Report: Primary Brain Tumors in the Unites states 1998 2002, the Central Brain Tumor Registry of the United States; 2006.

Chang EL, Loeffler JS, Riese NE, Wen PY, Alexander E, Black PM, Coleman CN. Survival results from a phase I study of etonidazole and radiotherapy in patients with malignant glioma. Int J Radiat Oncol Biol Phys 40: 65–70; 1998.

DeAngelis LM: Brain tumors. N Engl J Med 344:114–123; 2001.

Doolittle ND, Miner ME, Hall WA et al. Safety and efficacy of a multicenter study using intra-aterial chemotherapy in conjunction with osmotic opening of the blood-brain barrier for the treatment of patients with malignant brain tumors. Cancer 88(3):637-647; 2000.

Dougherty TJ, Gomer CJ, Henderson BW, Jori G, Kessel D, Korbelik M, Moan J, Peng Q. Photodynamic therapy. J Natl Cancer Inst. 90(12):889–905; 1998.

Dumont DJ, Yamaguchi TP, Conlon RA, Rossant J, Breitman ML. tek, a novel tyrosine kinase gene located on mouse chromosome 4, is expressed in endothelial cells and their presumptive precursors, Oncogene 7, 1471– 1480; 1992.

Ennis SR, Novotny A, Xiang J, Shakui P, Masada T, Stummer W, Smith DE, Keep RF. Transport of 5-aminolevu-linic acid between blood and brain. Brain Research 959:226 – 234; 2003.

Fingar VH. Vascular effects of photodynamic therapy. J Clin Laser Med Surg. 14:323–328; 1996.

Gaspar LE, Fisher BJ, Macdonald DR, Leber DV, Halperin EC, Schold SC, Cairncross JG. Supratentorial malignant glioma: Patterns of recurrence and implications for external beam local treatment. Int J Radiat Oncol Biol Phys 24: 55–57; 1992.

Gibson, SL, My Lien Nguyen, James J. Havens, Ayana Barbarin, Russell Hilf Relationship of δ-Aminolevulinic Acid-Induced Protoporphyrin IX Levels to Mitochondrial Content in Neoplastic Cells in Vitro; Biochemical and Biophysical Research Communications Vol. 265, 315–321; 1999.

Harrison BE, Johnson JL, Clough RW, Halperin EC. Selection of patients with melanoma brain metastases for aggressive treatment. American Journal of Clinical. American Journal of Clinical. Oncology. 26(4):354-357; 2003

Hasan T, Anne C.E. Moor, Bernard Ortel Photodynamic Therapy of Cancer; Principles of Radiation Oncology pp. 589-502; 2003.

Hill JS, Kahl SB, Kaye AH, Stylli SS, Koo MS, Gonzales MF, Vardaxis NJ, Johnson CI. Selective tumor uptake of a boronated pophyrin in an animal model of cerebral glioma. Proc Natl Acad Sci USA 89: 1785–1789; 1992.

Hill JS, Kaye AH, Sawyer WH, Morstyn G, Megison PD, Stylli SS. Selective uptake of haematoporphyrin derivative into human cerebral glioma. Neurosurgery 26: 248–254; 1990.

Hirschberg H, Mathews MS, Angell-Petersen E, Spetalen S, Madsen SJ. Increased brain edema following 5-aminolevulinic acid administration mediated photodynamic therapy in normal and tumor-bearing rats. Proc SPIE 6424:64242B1-8; 2007.

Hirschberg H, Michelle Zhang, David Chighvinadze, Qian Peng, and Steen J. Madsen, "Targeted opening of the blood brain barrier by ALA mediated PDT," Proceedings SPIE, vol. 6842, Photonic Therapeutics and Diagnostics IV, N. Kollias et al. (Eds.), in press.

Hori S, Ohtsuki S, Hosoya K, Nakashima E, Terasaki T. A pericyte-derived angiopoietin-1 multimeric complex induces occludin gene expression in brain capillary endothelial cells through Tie-2 activation in vitro, J. Neurochem. 89, 503–513; 2004.

Hu SS, Cheng HB, Zheng YR, Zhang RY, Yue W, Zhang H. Effects of photodynamic therapy on the ultrastructure of glioma cells. Biomed Environ Sci. 20(4):269-73; 2007

Ito S, Rachinger W, Stepp H, Reulen HJ, Stummer W, Oedema formation in experimental photo-irradiation therapy of brain tumours using 5-ALA. Acta Neurochir (Wien) 147: 57–65; 2005.

Iwama A, Hamaguchi I, Hashiyama M, Murayama Y, Yasunaga K, Suda T. Molecular cloning and characterization of mouse TIE and TEK receptor tyrosine kinase genes and their expression in hematopoietic stem cells, Biochem. Biophys. Res. Commun. 195, 301–309; 1993.

Kaal EC, Vecht CJ. The management of brain edema in brain tumors, Curr. Opin. Oncol. 16, 593–600; 2004.

Kaye AH, Morstyn G, Apuzzo M. Photoradiation therapy and its potential in the management of neurosurgical tumors, a review. J Neurosurg 68: 1–14; 1988.

Lee SW, Kim WJ, Choi YK, Song HS, Son MJ, Gelman IH, Kim YJ, Kim KW. SSeCKS regulates angiogenesis and tight junction formation in blood– brain barrier, Nat. Med. 9, 900–906; 2003.

Madsen SJ, et al. Journal of Environmental Pathology, Toxicology and Oncology 26(2); 2007.

Madsen SJ, Even Angell-Petersen, Signe Spetalen, Stephen W Carper, Sarah A Ziegler, and Henry Hirschberg. Photodynamic Therapy of Newly Implanted Glioma Cells in the Rat Brain: Lasers Surg Med 38:540 – 548; 2006.

Madsen SJ, Sun C-H, Tromberg BJ, Hirschberg H. Development of a novel balloon applicator for optimizing light delivery in photodynamic therapy. Lasers Surg Med 29:406-412; 2001.

Maisonpierre PC, Suri C, Jones PF, Bartunkova S, Wiegand SJ, Radziejewski C, Compton D, McClain J, Aldrich TH, Papadopoulos N, Daly TJ, Davis S, Sato TN, Yancopoulos GD. Angiopoietin-2, a natural antagonist for Tie2 that disrupts in vivo angiogenesis, Science 277, 55–60; 1997.

McGillion FB, Thompson GG, Goldberg A. Tissue uptake of delta-aminolevulinic acid. Biochem Pharmacol 24: 299 – 301; 1975.

McGillion FB, Thompson GG, Moore MR, Goldberg A. The passage of 5-aminolevulinic acid across the blood brain barrier of the rat—Effect of ethanol. Biochem Pharmacol 23:472 – 474; 1974.

Moan, J. & Berg, K. The photodegradation of porphyrins in cells can be used to estimate the lifetime of singlet oxygen. Photochem. Photobiol 53, 549–553; 1991.

Muller PJ, Wilson BC. An update on the penetration depth of 630 nm light in normal and malignant human brain tissue in vivo. Phys Med Biol 31: 1295–1297; 1986.

Nag S, Papneja T, Venugopalan R, Stewart DJ. Increased angiopoietin2 expression is associated with endothelial apoptosis and blood–brain barrier breakdown, Lab. Invest. 85, 1189–1198; 2005.

Pardridge WM. Drug and gene delivery to the brain: The vascular route. Neuron 36:555-558; 2002.

Pardridge WM. Drug and gene targeting to the brain with molecular Trojan horses. Nat Rev Drug Discov. 1:131-139; 2002.

Peng Q, Warloe T, Berg K. Clinical 5-Aminolevulinic Acid-Based Photodynamic Therapy. Cancer 79(12); 1997.

Senger DR, Galli SJ, Dvorak AM, Perruzzi CA, Harvey VS, Dvorak HF. Tumor cells secrete a vascular permeability factor that promotes accumulation of ascites fluid, Science 219, 983–985; 1983.

Shanley BC, Percy VA, Neethling AC. Neurochemistry of acute porphyria. In: Doss M, editor. Porphyrins in human diseases: Proceedings of the 1st international porphyrin meeting. Basel: S. Karger AG. pp. 152 – 162; 1975.

Singhal BS.Corticosteroids in the treatment of multiple sclerosis. Oger J. Multiple sclerosis, Demos Medical Publishing, LLC. Ch 6. Pp 59-64; 2006.

Sipos L, Vitanovics D, Afra D. Treatment of recidive malignant gliomas with temozolomide. Orv Hetil 143(21):1201–1204; 2002.

Snyder JW, Greco WR, Bellnier DA, Vaughan L, Henderson BW. Photodynamic Therapy: A Means to Enhanced Drug Delivery to Tumors. Cancer Res 63: 8126–8131; 2003.

Sporn LA, Foster TH. Photofrin and light induces microtubule depolymerization in cultured human endothelial cells. Cancer Res 52:3443–3448; 1992.

Stummer W, Tobias Beck, Wolfgang Beyer, Jan Hendrik Mehrkens, Andreas Obermeier, Nima Etminan, Herbert Stepp, Jörg-Christian Tonn, Reinhold Baumgartner, Jochen Herms, Friedrich Wilhelm Kreth. Long-sustaining response in a patient with non-resectable, distant recurrence of glioblastoma multiforme treated by interstitial photodynamic therapy using 5-ALA: case report. J Neuro Oncol 87:103–109; 2008.

Svaasand LO, Ellingsen R. Optical penetration in human intracranial tumors. Photochem photobiol 41: 73–76; 1985.

Walker MD, Alexander E, Hunt WE, et al. Evaluation of BCNU and/or radiotherapy in the treatment of anaplastic gliomas. A cooperative clinical trial. J Neurosurg 49:333–343; 1978.

Walker MD, Green SB, Byar DP, et al. Randomized comparisons of radiotherapy and nitrosoureas for the treatment of malignant gliomas after surgery. N Engl J Med 303:1323–1329; 1980.

Wallner KE, Galicich JH, Krol G, Arbit E, Malkin MG. Patterns of failure following treatment for glioblastoma multi- forme and anaplastic astrocytoma. Int J Radiat Oncol Biol Phys 16: 1405–1409; 1989.

Weis SM, Cheresh DA. Pathophysiological consequences of VEGF-induced vascular permeability, Nature 437, 497–504; 2005.

Wilson BS, Jeeves WP, Lowe DM. Light propagation in animal tissue in the wavelength range 375–825 nanometers. In: Dorion DR, Gomer CJ (eds) Prophyrin localisation and treatment of tumors. Alan R Liss, New York, pp 115–132; 1984.

Yancopoulos GD, Davis S, Gale NW, Rudge JS, Wiegand SJ, Holash J. Vascular-specific growth factors and blood vessel formation, Nature 407, 242–248; 2000.

Yung WK, Albright RE, Olson J, Fredericks R, Fink K, Prados MD, Brada M, Spence A, Hohl RJ, Shapiro W, Glantz M, Greenberg H, Selker RG, Vick NA, Rampling R, Friedman H, Phillips P, Bruner J, Yue N, Osoba D, Zaknoen S, Levin VA. A phase II study of temozolomide vs. procarbazine in patients with glioblastoma multiforme at first relapse. Br J Cancer 83:588–593; 2000.

VITA

Graduate College
University of Nevada, Las Vegas

David Chighvinadze

Local Address:
4201 S Decatur Blvd Apt 3183
Las Vegas, Nevada 89154

Home Address:
4930 W Hidden Valley Drive
Reno, Nevada 89502

Degrees:

Bachelor of Sciences, Physics, 2003
Ivane Javakhishvili State University of Tbilisi, Republic of Georgia

Master of Sciences, Physics, 2005
Ivane Javakhishvili State University of Tbilisi, Republic of Georgia

Publications:

Hirschberg H, Peng Q, Uzal FA, Chighvinadze D, Zhang MJ, Madsen SJ. "Disruption of the blood brain barrier following ALA mediated photodynamic therapy". Proceedings SPIE. Photonic Therapeutics and Diagnostics IV, N. Kollias et al. (Eds.) vol. 6842, pp-6842 20; 2008.

Hirschberg H, Uzal FA, Chighvinadze D, Zhang M, Peng Q, and Madsen SJ. "Disruption of the blood brain barrier following ALA mediated photodynamic therapy". Lasers in Surgery and Medicine; 2008.

Thesis Title: Evaluation of photodynamic therapy-induced edema in the rat brain using magnetic resonance imaging

Thesis Examination Committee:

Chairperson, Dr. Steen J. Madsen, Ph. D.
Committee Member, Dr. Phillip W. Patton, Ph. D.
Committee Member, Dr. Henry Hirschberg MD, Ph.D
Graduate Faculty Representative, Dr. Merrill Landers, DPT, OCS